

GRASP: GRaph-Structured Pyramidal Whole Slide Image Representation

Ali Khajegili Mirabadi¹Graham Archibald¹Amirali Darbandsari¹Alberto Contreras-Sanz^{1,2}Ramin Ebrahim Nakhli¹Maryam Asadi¹Allen Zhang¹C. Blake Gilks²Peter Black²Gang Wang³Hossein Farahani¹Ali Bashashati¹

{ali.mirabadi, ali.bashashati}@ubc.ca

¹The University of British Columbia, ²Vancouver Prostate Centre, ³BC Cancer

Abstract

Cancer subtyping is one of the most challenging tasks in digital pathology, where Multiple Instance Learning (MIL) by processing gigapixel whole slide images (WSIs) has been in the spotlight of recent research. However, MIL approaches do not take advantage of inter- and intra-magnification information contained in WSIs. In this work, we present GRASP, a novel graph-structured multi-magnification framework for processing WSIs in digital pathology. Our approach is designed to dynamically emulate the pathologist’s behavior in handling WSIs and benefits from the hierarchical structure of WSIs. GRASP, which introduces a convergence-based node aggregation instead of traditional pooling mechanisms, outperforms state-of-the-art methods over two distinct cancer datasets by a margin of up to 10% balanced accuracy, while being 7 times smaller than the closest-performing state-of-the-art model in terms of the number of parameters. Our results show that GRASP is dynamic in finding and consulting with different magnifications for subtyping cancers and is reliable and stable across different hyperparameters. The model’s behavior has been evaluated by two expert pathologists confirming the interpretability of the model’s dynamic. We also provide a theoretical foundation, along with empirical evidence, for our work, explaining how GRASP interacts with different magnifications and nodes in the graph to make predictions. We believe that the strong characteristics yet simple structure of GRASP will encourage the development of interpretable, structure-based designs for WSI representation in digital pathology. Furthermore, we publish two large graph datasets of rare Ovarian and Bladder cancers

to contribute to the field.

1. Introduction

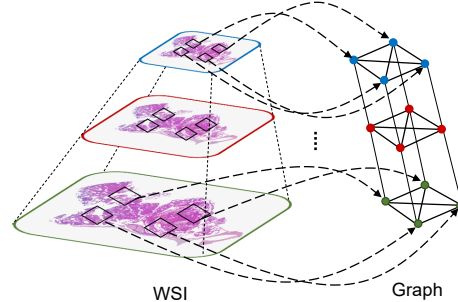


Figure 1. Representing a multi-magnification WSI via a hierarchical graph can capture inter- and intra-magnification information

Though deep learning has revolutionized computer vision in many fields, digital pathology tasks such as cancer classification remain a complex problem in the domain. For natural images, the task usually relates to assigning a label to an image with an approximate size of 256×256 pixels, with the label being clearly visible and well-represented in the image. Gigapixel tissue whole-slide images (WSIs) break this assumption in digital pathology as images exhibit enormous heterogeneity and can be as large as $150,000 \times 150,000$ pixels. Further, labels are provided at the slide level and may be descriptive of a small region of pixels occupying a minuscule portion of the total image, or they may be descriptive of complex interactions between the substructures within the entire composition of the WSI [9, 28, 20].

Multiple Instance Learning (MIL) has become the prominent approach to address the computational complexity of WSI; however, the majority of methods in the literature focus only on a single level of magnification, usually $20\times$ [18, 15, 23, 29, 5, 25, 30, 10]. Using this magnification, a set of patches from each WSI are extracted and used as an instance-level representation. This neither captures the biological structure of the data nor does it follow the diagnostic protocols of pathologists. That is to say, WSIs at higher magnifications contain additional details about the cell nucleus and intra- and extra-cellular matrix, while at lower magnifications one might discern the presence of blood vessels, connective tissue, or muscle fibers. Further, these structures are inconsistent from patient to patient, slide to slide, and subtype to subtype [19]. To capture this variability, pathologists generally use a variety of lenses in their inspection of a tissue sample under the microscope, switching between different magnifications as needed. They generally begin with low magnifications to identify regions of interest for making preliminary decisions before increasing magnifications to confirm or rule out diagnoses [21].

To address this challenge, several multi-magnification approaches have recently been introduced for different tasks of cancer subtyping, survival analysis, and image retrieval, though they are hindered as they often possess millions of parameters [26, 17, 22, 4, 8, 11].

In this research, we aim to further the progress of deep learning in this context by leveraging graph convolutional neural networks (GCNs) [16] with a multi-magnification component as they have been shown to capture more comprehensive and interpretable histopathologic information relating to the underlying mechanisms of a disease [1]. To this end, we introduce GRAPh-Structured Pyramidal (GRASP) WSI representation and use two different datasets, Ovarian Carcinoma and Bladder Cancer, to evaluate the model. Our main novelty and contributions include:

1. Introducing GRASP to capture pyramidal information contained in WSIs, as the first multi-magnification graph-structured model which integrates the concept of *zoom-in* as well as *zoom-out* into its structure.
2. Despite other multi-magnification approaches, GRASP benefits from a structural convergence instead of traditional pooling layers to capture inter-magnification information.
3. We provide a solid theoretical foundation of the model's functionality and its interpretability from both technical and pathological perspectives, as well as providing empirical evidence for the model's efficacy concerning hyperparameters.
4. We also publish two large datasets of rare cancers containing 948 graphs and WSIs for Ovarian Carcinoma and 262 graphs for Bladder Cancer. The code and the datasets are publicly available at **anonymized**.

2. Related Work

2.1. Patch-Level Encoding

With recent progress in deep learning, deep features, i.e. high-level embeddings from a deep network, have advanced past handcrafted features and are considered the most robust sources for image representation. Unfortunately, pre-trained networks such as DenseNet [14] or ResNet [12] draw their features from millions of non-medical and non-histopathological images, where they cannot necessarily produce high-level embeddings for complex images, especially rare cancers [27, 22, 6]. In this context, the use of Variational Autoencoders (VAEs) has been evaluated in [3], where the authors show that DenseNet pre-trained on ImageNet performs better for extracting semantic features from WSIs than VAEs. However, KimiaNet [22] was developed by employing the architecture of DenseNet with four dense blocks trained on a large set of pseudo-annotated histopathology images (patches) outperforming its pre-trained version on ImageNet.

2.2. Weak Supervision in Gigapixel WSIs

MIL Approaches: Several domains of deep learning have been explored in an attempt to effectively address the task of classification in digital pathology. Models such as AB-MIL [15], CLAM [18], and Trans-MIL [25] have utilized MIL with promising results. Such approaches have generally focused only on instance-level feature extraction and have not yet explored modeling global, long-range interactions within and across different magnifications.

Graph-based Approaches: To incorporate contextual information and long-range interactions, models such as PatchGCN [5] and DGCN [29] have been designed with a graph structure that can capture and learn context-aware features from interactions across the WSI. These models represent WSIs as graphs where the nodes are usually embeddings and edges are defined based on clustering or neighborhood node similarity, which in turn adds new hyperparameters and increases inference time. The similarity between nodes can be measured in terms of spatial or latent space, leading to the construction of different graphs for each WSI.

Multi-Magnification Approaches: Multiple efforts have been made to incorporate multi-magnification information in the context of gigapixel histopathology subtyping tasks. Models such as ZoomMIL [26], CSMIL [7], H^2 -MIL [13], and DSMIL [17] address this by aggregating contextual tissue information using features from multiple magnifications in WSIs. DSMIL concatenates embeddings from different magnifications together by duplicating lower-magnification features, making the model biased toward lower magnifications and unable to look into inter-magnification information. On the other hand, ZoomMIL aggregates information from $5\times$ to $20\times$ in a fixed hierarchy with no interaction in the

opposite direction. Chen et. al explore this in the context of vision transformers with their Hierarchical Image Pyramid Transformer (HIPT) [4]. Their architecture incorporates regions of size 256×256 and 4096×4096 pixels to leverage the natural hierarchical structure of WSIs. The aforementioned methods result in millions of parameters, which leads to highly complex and less interpretable models. H^2 -MIL also adopts a graph-based approach, where it pools the nodes in each magnification using an Iterative Hierarchical Pooling module. Our proposed model, on the other hand, is designed to dynamically aggregate information within and across different magnifications without using traditional pooling layers in its inter-magnification interactions.

3. Method

This section introduces the GRAPh-Structured Pyramidal (GRASP) WSI Representation, a framework for subtype recognition using multi-magnification weakly-supervised learning, illustrated in Figure 2.

3.1. Problem Formulation

Contrary to Multiple Instance Learning (MIL) approaches, which use a bag of instances to represent a given WSI, GRASP benefits from a graph-based, multi-magnification structure to objectively represent connections between different instances across and within different magnifications. To build a graph and learn a graph-based function \mathcal{F} that predicts slide-level labels with no knowledge of patch labels, the following formulation is adopted.

For a given WSI, $W_r \in \mathbb{R}^{N \times M \times 3}$ with label \mathcal{Y} , three sets of m patches, $\{p_i \in \mathbb{R}^{n \times n \times 3} : \forall i \in [1, \dots, m]\}$, $\{p'_i \in \mathbb{R}^{n \times n \times 3} : \forall i \in [1, \dots, m]\}$, and $\{p''_i \in \mathbb{R}^{n \times n \times 3} : \forall i \in [1, \dots, m]\}$ are extracted for each magnification of $\mathbf{M}_1 = 5x$, $\mathbf{M}_2 = 10x$, and $\mathbf{M}_3 = 20x$, respectively. It is important to note that p''_i is the high-resolution window located at the center of p'_i , and p'_i is the high-resolution window located at the center of p_i . *More details are provided in Patch Extraction in Supplementary Materials.*

These patches provide $3m$ patches in total that are then fed into an encoder ϕ , KimiaNet, to encode extracted patches into a lower dimension space as follows:

$$\phi : p_i \longrightarrow h_i \in \mathbb{R}^{d \times 1}, \forall i \in [1, \dots, m] \quad (1)$$

where h_i is the feature vector corresponding to the patch p_i . Correspondingly, h'_i represents p'_i , and so h''_i does p''_i . Using all the feature vectors for each W_r , graph \mathbb{G}_r is constructed using the transformation Γ :

$$\Gamma : \begin{bmatrix} \{h_1, \dots, h_m\} \\ \{h'_1, \dots, h'_m\} \\ \{h''_1, \dots, h''_m\} \end{bmatrix} \in \mathbb{R}^{3m \times d \times 1} \longrightarrow \mathbb{G}_r = (V_r, E_r) \quad (2)$$

Eventually, classifier \mathcal{C} is applied on top of graph convolutional layers \mathcal{G} to build the graph-based function \mathcal{F} to predict slide-level label \mathcal{Y} as follows:

$$\mathcal{Y} = \mathcal{F}(W_r) = \mathcal{C}(\mathcal{G}(V_r, E_r)) \quad (3)$$

3.2. GRASP

We start by extracting multi-magnification patches as described earlier. Then, for any i , we use the same encoder to encode p_i , p'_i , and p''_i into features h_i , h'_i , and h''_i respectively. Having instances features, we use the transformation Γ to build \mathbb{G}_r as introduced in Eq. 2.

The mechanism of connecting every two nodes in \mathbb{G}_r through Γ is premised upon an intuition of the pyramidal nature of WSIs as well as the way in which a conventional light microscope works when one switches from one magnification to another. When using a microscope, increasing magnification preserves the size of the image yet increases resolution by showing the central window of the lower magnification. This is the exact procedure we use to extract our patches in three magnifications. Therefore, for any i , h_i , h'_i , and h''_i are connected to each other via undirected edges, where this connection represents intra-magnification information contained in the features. On the other hand, for any i , all h_i 's contain information in \mathbf{M}_1 , such that they are connected to each other, forming a fully connected graph at \mathbf{M}_1 magnification to represent inter-magnification information. Similarly, all h'_i 's are connected to each other and also all the h''_i 's to represent inter-magnification information contained in \mathbf{M}_2 and \mathbf{M}_3 , respectively.

Figure 2 shows a small example of such a graph for $\mathbb{G}_r = (V_r, E_r)|_{m=4}$ where blue, red, and green nodes each form a fully connected graph of size m ; the intra-magnification relationship can also be seen via the edges between blue & red nodes as well as the red & green nodes. So far, each WSI, W_r , has been represented by graph \mathbb{G}_r with $3m$ nodes and $\frac{(3m+1)m}{2}$ edges. These graphs are thus deployed to train the GCNs and predict the label \mathcal{Y} at the output.

3.3. Graph Convolutional Layers

Following Eq. 3, we are defining \mathcal{G} which includes three GCN layers. The intuition behind using three layers is that as a pathologist begins to look for a tumor in a given WSI, they use an initial magnification to find the region of interest; Once found, they consult with other magnifications to confirm their decision since the data is complicated and often confusing. Therefore, as shown in Figure 2, all nodes in the graph interact with one another in a hierarchical fashion through the GCN layers. Consequently, each node gradually gathers information from all other nodes, and therefore, if there are any important messages carried by some nodes, it is guaranteed to be broadcast to all other nodes. This dynamic and hierarchical structure imposes theoretical properties on

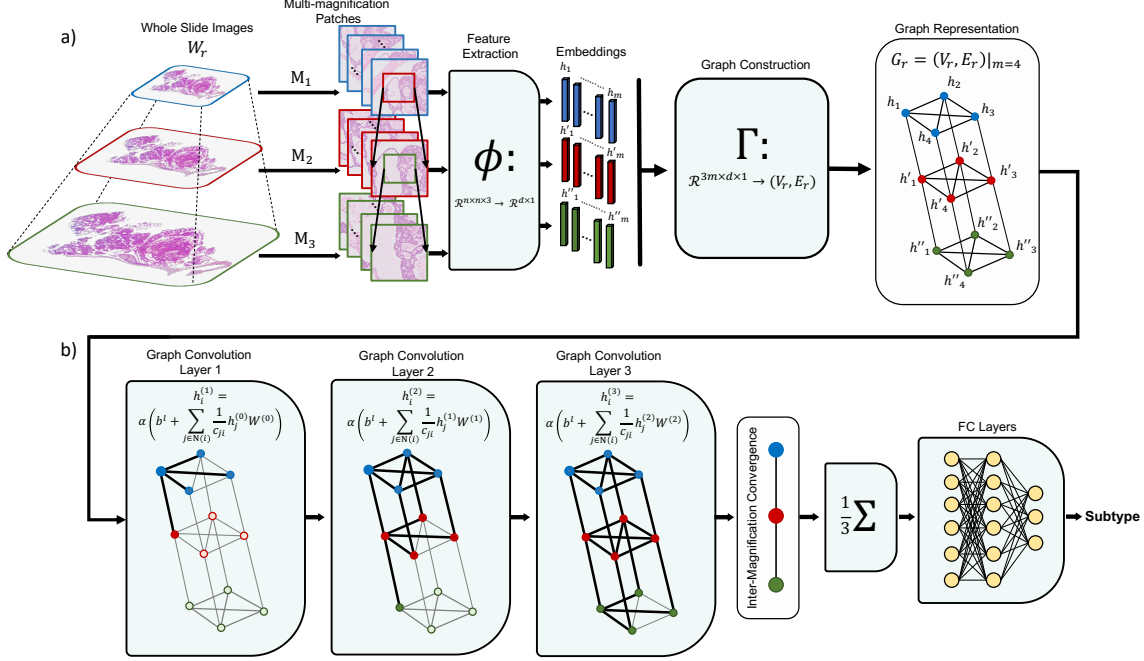


Figure 2. Overview of our workflow beginning with WSIs and outputting slide-level subtype predictions. **a)** shows the WSI being tiled into patches of varying magnification which are then embedded and assembled into a hierarchical graph. In **b)**, graph representations are fed into a three-layer GCN and subsequently, a two-layer MLP to predict graph-level (slide-level) subtypes. As shown in the message passing steps in **b)**, nodes in the first GCN layer interact with their immediate neighbors; those in the second GCN layer can interact with their second neighbors; and nodes in the final GCN layer can interact with all nodes in the graph. Then, the inter-magnification convergence causes the nodes within each magnification to converge, which is an intrinsic property of the architecture. In the end, the three converged nodes are passed through an average readout module. This dynamic helps the model to look for important messages in the entire graph, and if a node contains important information, it will be broadcast to all other nodes in the graph. The output of the GCN layers is then averaged by the *readout module* and passed to the FC layers. (For the sake of illustration, $m = 4$ is used to show the structure of GRASP).

the model which is going to be discussed here. Following the graph convolutional layer introduced in [16], the graph nodes are updated as follows:

$$h_i^{(l+1)} = \alpha(b^{(l)} + \sum_{j \in \mathcal{N}(i)} \frac{1}{c_{ji}} h_j^{(l)} W^{(l)}) \quad (4)$$

where $b^{(l)}$ is bias; $h_i^{(l+1)}$ is the node feature's update of the graph at $(l+1)$ -th step at \mathbf{M}_1 ; $\mathcal{N}(i)$ is the set of neighbors of node i , $c_{ji} = \sqrt{|\mathcal{N}(j)| |\mathcal{N}(i)|}$, where given the symmetry of the graph, all c_{ji} s are equal; and $\alpha(\cdot)$ is the activation function, which is ReLU in our implementation. $h_i^{(l+1)}$ and $h_i''^{(l+1)}$ expressions follow the same logic as $h_i^{(l+1)}$ in terms of the parameters mentioned above.

After the last graph convolutional layer, where the inter-magnification convergence happens, the graph is passed through an average readout module to pool the three-node graph mean embedding and then it is fed into the two-layer classifier \mathcal{C} to predict \mathcal{Y} .

3.4. Inter-Magnification Convergence

Based on the idea of distilling the information within and across magnifications to capture inter- and intra-magnification information, we now show that node features are converging in each magnification in the model. Having this, GRASP essentially encodes a graph of size $3m$ nodes to only 3 nodes. We interpret this as the model learning the information contained in the magnification through interaction with other magnifications.

Theorem 1 *Supposing the graph convolutional layers have L_2 -bounded weights, and the graph node features at $l = 0$ are L_2 -bounded. Therefore, $\forall i, j \in [1, \dots, m]$,*

$$\begin{aligned} \lim_{m \rightarrow \infty} \|h_i^{(3)} - h_j^{(3)}\|_2 &= 0; \quad \lim_{m \rightarrow \infty} \|h_i'^{(3)} - h_j'^{(3)}\|_2 = 0; \\ \text{and } \lim_{m \rightarrow \infty} \|h_i''^{(3)} - h_j''^{(3)}\|_2 &= 0 \end{aligned} \quad (5)$$

Proof: Please see Inter-Magnification Convergence in Supplementary Materials.

Corollary 1 $\forall i \in [1, \dots, m]$ and m sufficiently large, $h_i^{(3)} \rightarrow h^*$, $h_i'^{(3)} \rightarrow h'^*$, and $h_i''^{(3)} \rightarrow h''^*$, where

h^* , h'^* , and h''^* are functions of m ; h^* , h'^* , and h''^* are the convergence node for each magnification.

Taking into account the fact that h^* , h'^* , and h''^* are not necessarily equal, our model is fusing node features in each magnification while it consults with other magnifications, and draw the conclusion via averaging nodes across three magnifications at the end of the convolutional layers by means of the readout module. This means that the final embedding of the graph is $\frac{h^* + h'^* + h''^*}{3}$. We believe that this process helps the model reduce variance and uncertainty in making predictions as m grows. To support this claim, we provide empirical evidence detailed in section *Monte Carlo Test*.

The structure of the graph has been designed in such a way that it does not get stuck in the bottleneck of over-smoothing, a common issue in deep GCNs [2]. Our intuition is that nodes in \mathbf{M}_1 , \mathbf{M}_2 , and \mathbf{M}_3 are interacting via message passing, and the flow of intra-magnification information helps the model to keep its balance and continue the process of learning. Nevertheless, by increasing the number of GCN layers for the model to four or higher, the so-called over-smoothing problem will take place, which can possibly deteriorate the model’s performance. On the other hand, less than three layers of GCNs might not be able to fully capture the intra-magnification interactions. This leaves us with three layers of GCNs, which is equal to the graph’s diameter. In addition to this theoretical description, we empirically support our claim: *please see Graph Depth in Supplementary Materials*.

4. Experiments

4.1. Data preparation

We use two datasets: Ovarian Carcinoma and Bladder Cancer, where the former consists of 948 WSIs with five histotypes including high-grade serous carcinoma (HGSC; 410), clear cell ovarian carcinoma (CCOC; 167), endometrioid carcinoma (ENOC; 237), low-grade serous carcinoma (LGSC; 69), and mucinous carcinoma (MUC; 65), and the latter consists of 262 WSIs with two histotypes including micropapillary (MicroP; 128) and conventional urothelial carcinomas (UCC; 134). A total of 1,133,388 patches of size 1000×1000 pixels for the Ovarian dataset and 313,191 patches of size 1000×1000 pixels for the Bladder dataset are extracted in multi-magnification mode (approximately 1.5 TB of Gigapixel WSIs). Patches being extracted such that they do not overlap at \mathbf{M}_3 while overlapping at \mathbf{M}_2 and \mathbf{M}_1 is inevitable. From each magnification, $m \leq 400$ patches have been extracted per slide, as it’s been shown in [3, 27, 21] that a subset of patches is enough to represent WSIs. For each cancer dataset, we trained our proposed method in a 3-fold cross-validation and repeated the experiments *ten* times with

different random seeds, where random seeds were randomly generated. In order to prevent data leakage in our cross-validation splits, we split the slides based on their patients, since some patients have more than one slide, meaning that slides were split in a way that all slides from the same patient remain in the same set. *More information is available in Supplementary Materials*.

4.2. Training and Inference

To tackle the data imbalance problem, for all models in the study, we deployed a weighted cross entropy loss. A learning rate of 0.001 and a weight decay of 0.01 for Adam optimizer have been adopted, and in case competing models were not converging, learning rate of 0.0001 resolved the problem. Models were trained for 100 epochs and 10 epochs for the Ovarian and the Bladder dataset, respectively. Specific to GRASP, the first two layers are of size 256 and the last layer output is of size 128. For all training and testing, the GPU hardware used was either a GeForce GTX 3090 Ti-24 GB (Nvidia) or Quadro RTX 5000-16 GB (Nvidia) based on availability. Deep Graph Library (DGL), PyTorch, NumPy, SciPy, PyGeometric, and Scikit-Learn libraries have been used to perform the experiments.

4.3. Comparisons with State-of-the-Art

To compare with state-of-the-art approaches, we repeated these experiments with the same cross-validation folds and random seeds to have a fair comparison; the choice of ten random seeds is to capture statistical significance and reliability. For evaluating the models, we adopt Balanced Accuracy and F1 Score since these metrics show how reliable a model performs on imbalanced data, and more importantly on clinical applications. We compare our proposed model, GRASP, with models using different approaches to have a broad spectrum of evaluation. These models include Ab-MIL [15], Trans-MIL [25], CLAM-SB [18], and CLAM-MB [18] from the attention/transformer-based family; ZoomMIL [26] from multi-magnification approaches since it has a hierarchical structure and is compatible with our patch extraction paradigm; and PatchGCN: latent & spatial [5] and DGCN: latent & spatial [29] from graph-based learning approaches.

4.4. Subtype Prediction

Table 1 shows the comparison between our model and state-of-the-art methods, where GRASP outperforms all the competing methods by a margin of 2.6% – 10.7% Balanced Accuracy on the Ovarian dataset and 0.4% – 10.0% on the Bladder dataset. It is worth mentioning that ZoomMIL is the closest-performing model to GRASP, although ZoomMIL has 7 times more parameters than GRASP. PatchGCN and DGCN are not performing comparably to GRASP, even though they are using spatial information that GRASP does not. This implies that a multi-magnification graph structure

Table 1. Average performance on 3 folds and 10 random seeds

Model	params.	inference	Ovarian: five subtypes		Bladder: two subtypes	
			Balanced Acc.	F1 Score	Balanced Acc.	F1 Score
Trans-MIL	2.672M	0.053 sec	0.647 ± 0.007	0.632 ± 0.005	0.868 ± 0.023	0.877 ± 0.013
Ab-MIL	0.263M	0.005 sec	0.692 ± 0.016	0.680 ± 0.014	0.919 ± 0.018	0.922 ± 0.016
CLAM-SB	0.795M	0.009 sec	0.627 ± 0.015	0.623 ± 0.010	0.908 ± 0.026	0.911 ± 0.023
CLAM-MB	0.796M	0.012 sec	0.620 ± 0.035	0.609 ± 0.030	0.901 ± 0.039	0.906 ± 0.037
DGCN: latent	0.790M	0.018 sec	0.654 ± 0.017	0.652 ± 0.024	0.835 ± 0.034	0.841 ± 0.035
DGCN: spatial	0.790M	0.030 sec	0.654 ± 0.009	0.652 ± 0.009	0.867 ± 0.015	0.875 ± 0.007
PatchGCN: latent	1.385M	0.018 sec	0.683 ± 0.003	0.675 ± 0.005	0.911 ± 0.031	0.919 ± 0.020
PatchGCN: spatial	1.385M	0.032 sec	0.672 ± 0.002	0.662 ± 0.005	0.896 ± 0.033	0.905 ± 0.021
ZoomMIL	2.891M	0.036 sec	0.701 ± 0.020	0.690 ± 0.021	0.931 ± 0.008	0.933 ± 0.009
GRASP (ours)	0.378M	0.005 sec	0.727 ± 0.036	0.689 ± 0.040	0.935 ± 0.011	0.937 ± 0.014

can potentially show more capability compared to other state-of-the-art approaches in terms of representing gigapixel WSIs. Moreover, GRASP and Ab-MIL have the lowest inference time, while GRASP is processing information in three magnifications and Ab-MIL is a single magnification model. Inference times (per slide) have been calculated on the same machine (RTX5000) for all models.

Although [7] has used attention score distribution to show their model is reliable across different magnifications, we want to step further and adopt a similar logic as first introduced in [24] to define the concept of energy of gradients for graph nodes (*More details in Supplementary Materials*). Therefore, for the first time in the field, we show that an AI model such as GRASP can learn the concept of magnification and behave according to the subtype and slide characteristics. To this end, we formulate an experiment to obtain a sense of each magnification’s influence on the model which leads to Figure 3. The main takeaway of this experiment is that depending on the subtype, the distribution of referenced magnifications by GRASP is different. From a pathological point of view, this finding fits our knowledge of the biological properties of each subtype. As an example, we conducted a case study on the bladder dataset, where the micropapillary subtype is known to be diagnosed generally in lower magnification owing to its morphological properties and the structure of micropapillary tumors, whereas UCC needs to be examined in higher magnifications due to its cell- and texture-dependent structure.

On the Ovarian dataset, for the subtype ENOC, endometrioids can often be recognized and identified at low power as they tend to have characteristic glandular architecture occupying contiguous, large areas. Low-grade serous carcinomas (LGSC) can be very difficult at low power due to the necessity of confirming low-grade cytology at high power. For CCOC, clear cell carcinomas have characteristic low-power architectural patterns but can also require high-power examinations to exclude high-grade serous carcinoma with clear cell features, meaning that important information is

distributed on all magnifications. The other subtypes, MUC and HGSC, may either show pathognomic architectural features at low power or require high-power examination on a case-by-case basis. According to Figure 3, GRASP collects the information from all three magnifications for MUC and CCOC.

4.5. Ablation Study

Here, we design two experiments to evaluate our proposed model. Firstly, a Monte Carlo test on graph size, i.e., the number of nodes. Secondly, analyzing model performance on individual or pairs of magnifications.

4.5.1 Monte Carlo Test

In this experiment, we take a graph of size $3m = 1200$, and randomly drop a set of its nodes, along with their multi-magnification correspondences, to build a new graph with a smaller size as described in Algorithm 1. For example, when $count = 10$, we randomly drop 10 triplets of $(h_{index}, h'_{index}, h''_{index})$ from the graph to create a new graph Q_r of the size 1170. Similarly, when $count = 200$, we randomly drop 200 triplets of $(h_{index}, h'_{index}, h''_{index})$ from the graph to create a new graph Q_r of the size 600. This is an aggressive way to create statistically independent graphs of smaller sizes. To capture statistical variance, we repeat the experiment 10 times to create 40 graphs with different sizes and report the model performance in Figure 4. To accomplish this, the same 3-fold cross-validation sets and 10 random seeds have been used for all repetitions. Taking 10 times repetitions of 40 different graph sizes into account, we performed 12,000 independent training and inference experiments. *See Monte Carlo Test in Supplementary Materials*.

As can be seen in Figure 4, the performance of GRASP increases and stabilizes as the number of nodes increases. Since the standard deviation decreases as the number of nodes increases, it brings to light the concept of variance convergence, meaning that the model with $m \geq 200$ is fairly

Magnification-Interaction Histogram

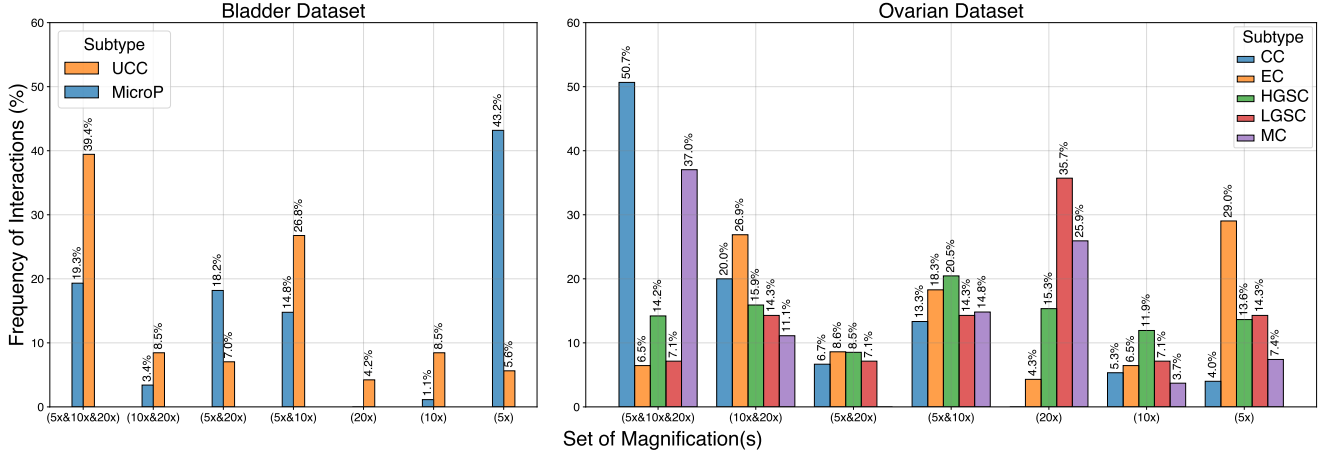


Figure 3. The histogram of consultations conducted by GRASP with different magnifications. First, this shows GRASP is actively dynamic in terms of capturing information from different magnifications benefiting from its multi-magnification structure. Second, information is distributed differently over magnifications depending on the subtype and slide, and there is no optimal magnification for a subtype. For example, in the Bladder dataset, ‘(5x&10x&20x)’ shows that the model needed to consult with all three magnifications for 19.3% and 39.4% of slides for MicroP and UCC, respectively; ‘(5x)’ shows that the model has mostly focused on only 5x magnification for 43.2% and 5.6% of slides for MicroP and UCC, respectively. This behavior is similar to pathologists, where they can diagnose massive MicroP tumors with lower magnifications, while they need to consult with higher magnifications for confirming a minuscule mass of MicroP tumors. On the other hand, UCC is hard to diagnose at lower magnifications and requires careful examination with different magnifications due to its morphological complexity, which fits the model behavior in proclivity to highlight more than one magnification for the majority of cases.

generalizable over different cross-validation folds and is statistically reliable in terms of performance. This is also in agreement with our theoretical expectation based on inter-magnification convergence that as m grows, the model has better convergence resulting in more stability.

Algorithm 1 Monte Carlo Test on Graph Size

```

Require:  $m = 400$ 
1:  $step \leftarrow 10$ 
2: Load DATASET
3:  $D \leftarrow \{\emptyset\}$  ▷ Node indices to be dropped
4: for 10 times do
5:   for  $G_r$  in DATASET do
6:     for  $count$  in  $[10 : step : 390]$  do
7:        $D \leftarrow \text{RANDOM}([1, \dots, m], count)$ 
8:        $Q_{r,count} \leftarrow G_r$ 
9:       for  $index$  in  $D$  do
10:         $Q_{r,count} \leftarrow \text{DROP}(Q_{r,count}, h_{index})$ 
11:         $Q_{r,count} \leftarrow \text{DROP}(Q_{r,count}, h'_{index})$ 
12:         $Q_{r,count} \leftarrow \text{DROP}(Q_{r,count}, h''_{index})$ 
13:      end for
14:      STORE( $Q_{r,count}$ )
15:    end for
16:  end for
17: end for
18: Take  $Q_{r,count}$  for Cross-Validation and Inference
report Balanced Accuracy & Standard Deviation

```

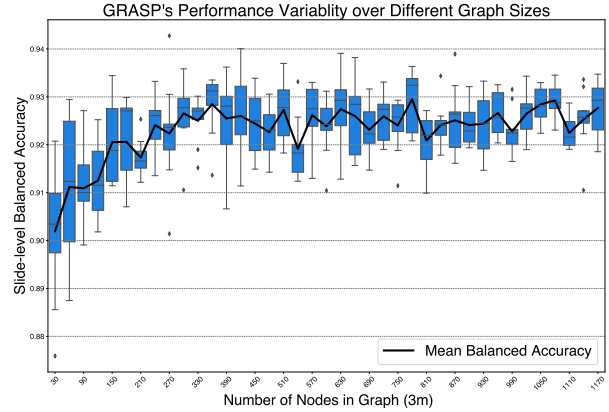


Figure 4. Monte Carlo experiment on the graph size.

4.5.2 Magnification Test

To confirm that the idea of multi-magnification is valid and that multi-magnification is the cause for the model’s performance, we design 6 different experiments (repeated on 10 random seeds and 3 folds) on the Bladder dataset as our empirical evidence. These include evaluating the same model on only M_1 , M_2 , and M_3 fully connected graphs and on pairs of $M_1 \& M_2$, $M_1 \& M_3$, and $M_2 \& M_3$. The results in Table 2 show that GRASP is superior to all other methods. One possible explanation is that for those single and paired graphs, three layers of GCNs most likely cause the aforementioned

Table 2. Average Performance on 3-folds and 10 random seeds

Model	Bladder Cancer	
	Balanced Acc.	F1 Score
Graph on M_1	0.898 ± 0.052	0.890 ± 0.047
Graph on M_2	0.927 ± 0.057	0.928 ± 0.051
Graph on M_3	0.905 ± 0.035	0.913 ± 0.023
Graph on $M_1 \& M_2$	0.919 ± 0.032	0.919 ± 0.030
Graph on $M_1 \& M_3$	0.917 ± 0.031	0.922 ± 0.033
Graph on $M_2 \& M_3$	0.926 ± 0.024	0.934 ± 0.022
GRASP (ours)	0.935 ± 0.011	0.937 ± 0.014

tioned over-smoothing problem, which shows that GRASP can effectively capture the information contained in different magnifications and boost its performance.

5. Conclusion

In this work, we developed GRASP, a graph-structured multi-magnification framework for processing gigapixel WSIs. GRASP is a *dynamic* model that can learn multi-magnification interactions in the data based on the idea of capturing both the inter- and intra-magnification information. This relies on the theoretical property of the model, where it benefits from inter-magnification convergence to pool the nodes rather than conventional pooling layers. GRASP, which has comparably fewer parameters than other state-of-the-art multi-magnification models in the field, outperforms all of the competing models in terms of *Balanced Accuracy* over two complex cancer datasets. For the first time in the field, confirmed by two expert genitourinary pathologists, we showed that our model is dynamic in finding and consulting with different magnifications for subtyping two challenging cancers. We also evaluated the model decision-making to show that the model is learning semantics by highlighting tumorous regions in patches. Furthermore, we not only run extensive experiments to show the model’s reliability and stabilization in terms of its different hyperparameters, but we also provide the theoretical foundation of our work to shed light on the dynamics of GRASP in interacting with different nodes and magnifications in the graph. To conclude, we hope that the strong characteristics of GRASP and its straightforward structure, along with the theoretical basis, will encourage the modeling of structure-based design in the field of digital pathology for WSI representation.

As part of potential future directions, GRASP’s performance on other clinical tasks such as survival analysis and outlier detection, and its potential to incorporate other biological modalities, especially those that are represented as graphs, into GRASP’s graph structure can be investigated.

References

- [1] David Ahmedt-Aristizabal, Mohammad Ali Armin, Simon Denman, Clinton Fookes, and Lars Petersson. A survey on graph-based deep learning for computational histopathology. *Computerized Medical Imaging and Graphics*, 95:102027, 2022.
- [2] Chen Cai and Yusu Wang. A note on over-smoothing for graph neural networks. *arXiv preprint arXiv:2006.13318*, 2020.
- [3] Chen Chen, Ming-Yuan Lu, David F. K. Williamson, Andrew D. Trister, Ravi G. Krishnan, and Faisal Mahmood. Fast and scalable search of whole-slide images via self-supervised deep learning. *Nature biomedical engineering*, 6(12):1420–1434, 2022.
- [4] Richard J Chen, Cheng Chen, Yuanfang Li, Tsung-Ying Chen, Andrew D Trister, Ravi G Krishnan, and Faisal Mahmood. Scaling vision transformers to gigapixel images via hierarchical self-supervised learning. In *Proceedings of the IEEE/CVF Conference on Computer Vision and Pattern Recognition*, pages 16144–16155, 2022.
- [5] Richard J Chen, Ming-Yuan Lu, Muhammad Shaban, Chi Chen, Ting-Yun Chen, David F Williamson, and Faisal Mahmood. Whole slide images are 2d point clouds: context-aware survival prediction using patch-based graph convolutional networks. In *Medical Image Computing and Computer Assisted Intervention—MICCAI 2021: 24th International Conference, Strasbourg, France, September 27–October 1, 2021, Proceedings, Part VIII*, pages 339–349. Springer, 2021.
- [6] Ozan Ciga, Tony Xu, and Anne Louise Martel. Self supervised contrastive learning for digital histopathology. *Machine Learning with Applications*, 7:100198, 2022.
- [7] Ruiqi Deng, Chun Cui, Lester W. Remedios, Shunxing Bao, Ryan M. Womick, Sylvain Chiron, Jialun Li, Joseph T. Roland, Keith S. Lau, Qing Liu, and Keith T. Wilson. Cross-scale multi-instance learning for pathological image diagnosis. *arXiv preprint arXiv:2304.00216*, April 2023.
- [8] Timothy M D’Alfonso, David J Ho, Matthew G Hanna, Zhi Li, Hongyan Li, Limei Tang, Lei Zhang, Ziyang Li, Ruiyang Liu, Yiming Zheng, et al. Multi-magnification-based machine learning as an ancillary tool for the pathologic assessment of shaved margins for breast carcinoma lumpectomy specimens. *Mod Pathol*, 34:1487–1494, 2021.
- [9] Babak Ehteshami Bejnordi, Mitko Veta, Paul Johannes van Diest, and et al. Diagnostic assessment of deep learning algorithms for detection of lymph node metastases in women with breast cancer. *JAMA*, 318(22):2199–2210, 2017.
- [10] Yonghang Guan, Jun Zhang, Kuan Tian, Sen Yang, Pei Dong, Jinxi Xiang, Wei Yang, Junzhou Huang, Yuyao Zhang, and Xiao Han. Node-aligned graph convolutional network for whole-slide image representation and classification. In *2022 IEEE/CVF Conference on Computer Vision and Pattern Recognition (CVPR)*, pages 18791–18801, 2022.
- [11] Noriaki Hashimoto, Daisuke Fukushima, Ryoichi Koga, Yusuke Takagi, Kaho Ko, Kei Kohno, Masato Nakaguro, Shigeo Nakamura, Hidekata Hontani, and Ichiro Takeuchi. Multi-scale domain-adversarial multiple-instance cnn for cancer subtype classification with unannotated histopathological

- images. In *Proceedings of the IEEE/CVF Conference on Computer Vision and Pattern Recognition (CVPR)*, June 2020.
- [12] Kaiming He, Xiangyu Zhang, Shaoqing Ren, and Jian Sun. Deep residual learning for image recognition. In *Proceedings of the IEEE conference on computer vision and pattern recognition*, pages 770–778, 2016.
- [13] Wenjin Hou, Lu Yu, Chao Lin, Heng Huang, Rongtao Yu, Jing Qin, and Liang Wang. H²-mil: Exploring hierarchical representation with heterogeneous multiple instance learning for whole slide image analysis. In *Proceedings of the AAAI Conference on Artificial Intelligence*, volume 36, pages 933–941, 2022.
- [14] Gao Huang, Zhuang Liu, Laurens Van Der Maaten, and Kilian Q. Weinberger. Densely connected convolutional networks. In *Proceedings of the IEEE Conference on Computer Vision and Pattern Recognition*, pages 4700–4708. IEEE, 2017.
- [15] Maximilian Ilse, Jakob Tomczak, and Max Welling. Attention-based deep multiple instance learning. In *International Conference on Machine Learning*, pages 2123–2132. PMLR, 2018.
- [16] Thomas N. Kipf and Max Welling. Semi-supervised classification with graph convolutional networks. *arXiv preprint arXiv:1609.02907*, 2016.
- [17] Bin Li, Yin Li, and Kevin W. Eliceiri. Dual-stream multiple instance learning network for whole slide image classification with self-supervised contrastive learning. In *Proceedings of the IEEE/CVF Conference on Computer Vision and Pattern Recognition*, pages 14318–14328, 2021.
- [18] Michael Y. Lu, David F.K. Williamson, Tai-Yen Chen, and et al. Data-efficient and weakly supervised computational pathology on whole-slide images. *Nature Biomedical Engineering*, 5(6):555–570, 2021.
- [19] Anamarija Morovic, Perry Damjanov, and Kyle Perry. *Pathology for the Health Professions-Sixth Edition*. Elsevier Health Sciences, 2021.
- [20] Nick Pawlowski, Saurabh Bhooshan, Nicolas Ballas, Francesco Ciompi, Ben Glocker, and Michal Drozdal. Needles in haystacks: On classifying tiny objects in large images. *arXiv preprint arXiv:1908.06037*, 2019.
- [21] Maral Rasoolijaberi, Morteza Babaei, Abtin Riasatian, Sobhan Hemati, Parsa Ashrafi, Ricardo Gonzalez, and Hamid R. Tizhoosh. Multi-magnification image search in digital pathology. *IEEE Journal of Biomedical and Health Informatics*, 26(9):4611–4622, 2022.
- [22] Abtin Riasatian, Morteza Babaie, Danial Maleki, Shivam Kalra, Mojtaba Valipour, Sobhan Hemati, Mani Zaveri, Amir Safarpour, Sobhan Shafiei, Mehdi Afshari, Maral Rasoolijaberi, Milad Sikaroudi, Mohd Adnan, Sulmaan Shah, Charles Choi, Savvas Damaskinos, Clinton JV Campbell, Phedias Diamandis, Liron Pantanowitz, Hany Kashani, Ali Ghodsi, and H. R. Tizhoosh. Fine-tuning and training of densenet for histopathology image representation using tcga diagnostic slides, 2021.
- [23] Yoni Schirris, Efstratios Gavves, Iris Nederlof, Hugo Mark Horlings, and Jonas Teuwen. Deepsmile: Contrastive self-supervised pre-training benefits msi and hrd classification directly from h&e whole-slide images in colorectal and breast cancer. *Medical Image Analysis*, 79:102464, 2022.
- [24] Ramprasaath R. Selvaraju, Michael Cogswell, Abhishek Das, Ramakrishna Vedantam, Devi Parikh, and Dhruv Batra. Grad-cam: Visual explanations from deep networks via gradient-based localization. In *Proceedings of the IEEE International Conference on Computer Vision (ICCV)*, Oct 2017.
- [25] Zhuchen Shao, Hao Bian, Yang Chen, Yifeng Wang, Jian Zhang, Xiangyang Ji, and Yongbing Zhang. TransMIL: Transformer based correlated multiple instance learning for whole slide image classification. In A. Beygelzimer, Y. Dauphin, P. Liang, and J. Wortman Vaughan, editors, *Advances in Neural Information Processing Systems*, 2021.
- [26] Kevin Thandiackal, Boqi Chen, Pushpak Pati, Guillaume Jaume, Drew F. K. Williamson, Maria Gabrani, and Orcun Goksel. Differentiable zooming for multiple instance learning on whole-slide images. In Shai Avidan, Gabriel Brostow, Moustapha Cissé, Giovanni Maria Farinella, and Tal Hassner, editors, *Computer Vision – ECCV 2022*, pages 699–715. Cham, 2022. Springer Nature Switzerland.
- [27] Xiyue Wang, Yuexi Du, Sen Yang, Jun Zhang, Minghui Wang, Jing Zhang, Wei Yang, Junzhou Huang, and Xiao Han. Retccl: Clustering-guided contrastive learning for whole-slide image retrieval. *Medical Image Analysis*, 83:102645, 2023.
- [28] Xingyuan Zhang, Hang Su, Lin Yang, and Shuicheng Zhang. Fine-grained histopathological image analysis via robust segmentation and large-scale retrieval. In *2015 IEEE Conference on Computer Vision and Pattern Recognition (CVPR)*, pages 5361–5368, Boston, MA, USA, 2015.
- [29] Yu Zheng, Chen Gao, Liang Chen, Depeng Jin, and Yong Li. Dgcn: Diversified recommendation with graph convolutional networks. In *Proceedings of the Web Conference 2021, WWW '21*, page 401–412, New York, NY, USA, 2021. Association for Computing Machinery.
- [30] Yanning Zhou, Simon Graham, Navid Alemi Koohbanani, Muhammad Shaban, Pheng-Ann Heng, and Nasir Rajpoot. Cgc-net: Cell graph convolutional network for grading of colorectal cancer histology images. In *Proceedings of the IEEE/CVF International Conference on Computer Vision (ICCV) Workshops*, Oct 2019.